2021 43rd Annual International Conference of the
IEEE Engineering in Medicine & Biology Society (EMBC)
Oct 31 - Nov 4, 2021. Virtual Conference

Passive Rotation Angle Motion Validation for an Ankle-Foot Orthosis Multi-Jointed Surrogate Lower Limb Design

A. Thibodeau, P. Dumond, and E.D. Lemaire

Abstract— **Ankle-foot orthoses (AFO) are devices that assist lower limb motion. Mechanical testing an AFO would ideally load the device while worn on the leg, since AFO function is dependent on intimate leg contact. However, this is not appropriate for cyclic or load-to-failure applications. A surrogate lower limb (SLL) was designed for this AFO testing application, to provide anthropometric 3D movement when subjected to standard test loads. This novel four-joint SLL was inspired by the Rizzoli foot model, which segments the lower limb into five sections. SLL joint prototypes were validated by measuring rotation angles and comparing with typical anatomical ranges of motion. The 3D printed models were within acceptable variability of human joint movement and, therefore, were appropriate for use in the final SSL.**

Clinical Relevance— **A new surrogate lower limb provides 3D anatomically correct joint movements, not available in previous SLL designs. This device was designed to be affordable and easy to fabricate using readily available equipment, enabling more people to recreate and use the SLL for research or clinical measurement. This will enable appropriate AFO testing, especially for devices that allow non-planar movement.**

I. Introduction

Ankle-foot orthoses (AFO) assist individuals with problems controlling their lower limb. While many AFO designs exist [1], the principal goal is to control ankle rotation by providing additional stiffness to the joint. Several methods exist for testing AFO properties, including stiffness and range of motion (RoM) [2,3]. To represent human-AFO interactions using these testing methods, researchers created surrogate lower limbs (SLL). However, existing SLL designs, with only single axis ankle joints and no foot articulations prevent realistic lower limb motion [4,5].

The lower limb includes several interconnected joints. However, due to the surrounding tissues, some joint motions are heavily limited, while other joints have a high RoM. For biomechanical motion analysis, multi-segment foot models preserve essential rotations by segmenting the lower limb into rigid bodies [6]. The Rizzoli model reduces the lower limb to five segments by fusing several limited joints and preserving essential rotations [7]. These segments include the shank, hindfoot, midfoot, forefoot and hallux. The Rizzoli model provides the relative rotation angle of each joint in each three-dimensional plane [7].

The goal of this study was to design an improved SLL that replicates realistic 3D motions, thereby enabling mechanical evaluations of current AFO designs and guiding clinical prescription with quantitative evidence.

II. Design

The new SLL design, based on the Rizzoli model, includes five segments with four joints: shank-hindfoot (SH), hindfoot-midfoot (HM), midfoot-forefoot (MF), forefoot-toes (FT). The FT rotates only in the sagittal plane, while the SH, HM, and MF rotate in the frontal, sagittal and transverse planes (TABLE I). Three-dimensional joints use ball and socket connections, while the FT uses a hinge-type connector. Although anatomical joints have oblique axes, the SLL ball and socket joints do not have defined axes of rotation. However, Maximum range of motion in each direction is limited by specially designed angled surfaces on the foot segments. As such, these joints can easily replicate the combined rotation that would occur due to oblique axes, while remaining easy to fabricate. The shank combines a metal shaft surrounded by a cover 3D printed using fused deposition modeling (FDM). The foot components are printed using fatigue resistant nylon [8]. Thermoplastic polyurethane (TPU) is used to print flexible connectors between nylon components. The connectors allow rotation but provide some resistance to motion. Silicone rubber emulates the soft tissue and is moulded around the foot's nylon components based on the shape of a Össur™ FSTM26R prosthetic foot cover. The entire SLL and its components are shown in Fig. 1 and 2.

TABLE I. SLL Joint Rotation Angles

	SH	HM	MF	FT
Eversion	20.0°	3.5°	3.5°	-
Inversion	30.0°	3.2°	7.0°	-
Dorsiflexion	20.0°	2.2°	6.5°	80.0°
Plantarflexion	50°	2.2°	6.1°	30.0°
Abduction	-	0.5°	6.5°	-
Adduction	-	3.8°	2.0°	-

A. Thibodeau is with the university of Ottawa, ON, Canada (phone: 613-277-6413; e-mail: athib018@uottawa.ca).

P. Dumond is a Professor in Mechanical Engineering at the University of Ottawa (pdumond@uottawa.ca)

E.D. Lemaire is a Professor in Physical Medicine and Rehabilitation, an adjunct Professor in Mechanical Engineering and Human Kinetics at the University of Ottawa. Ottawa, ON Canada, and an Affiliate Investigator in the Clinical Epidemiology Program at the Ottawa Hospital Research Institute (elemaire@ohri.ca)

Figure 1. Overall SLL design

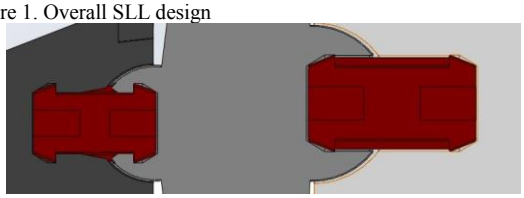

Figure 2. Cross-sectional view of the MF/HM annular connectors

A. Shank -Hindfoot Joint

The shank shaft's distal end has a threaded ball stud that sits in the heel base's superior socket. This socket is a semi-circular cup (Fig. 3a). The ball stud is locked in place using a sectioned plate that allows ball insertion. An opening on the top plate (Fig. 3b) controls the ball stud neck's maximum motion, providing anatomical rotation in all directions. Maximum dorsiflexion (DF) and eversion (EVE) occur simultaneously. Maximum plantarflexion (PF) and inversion (INV) also happen simultaneously. These combined rotations replicate subtalar and talocrural joint motion, which are linked together [9].

The two top plate halves are bolted to the heel base, preventing the ball stud from popping out. The bolts are secured via hex nuts. The ball socket is above the bolts to avoid interference between the shank shaft and the bolt heads. Not seen in the model shown in Fig. 1 are four elastic bands constraining SH transverse rotation and providing joint stiffness.

B. Hindfoot-Midfoot and Midfoot-Forefoot Joints

Ball and Sockets: The HM and MF joints use ball and socket connectors. The heel base anterior surface and forefoot posterior surface have sockets, while the midfoot distal and proximal surfaces have balls (Fig. 2). Joint motion occurs due to the ball sliding inside the socket while the annular flexible connector holding the ball and socket together bends. Tapered clearance is provided to the connector inside the socket, allowing the connector to bend without shearing. Rotation angles are constrained by angled surfaces on the distal and proximal midfoot sides, preventing the ball and socket from over-rotating. These angled surfaces control abduction (AB) to adduction (AD) and DF-PF rotations.

Eversion-Inversion: Guide pins, located above the ball and socket joints, on the heel base and midfoot, limit HM and MF frontal rotation (EVE-INV). The pins follow curved grooves on the connecting parts. These grooves widen along their length to ensure that the pins do not prevent motion in the sagittal or transverse planes.

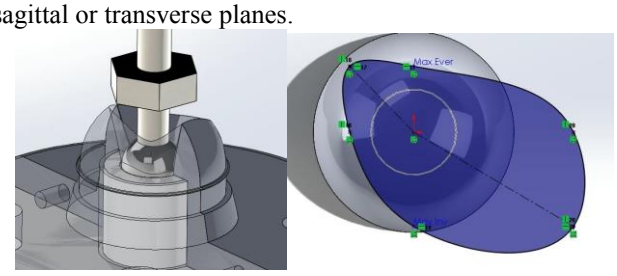

Figure 3. a) SH joint (left image), b) SH joint opening (right image)

Annular Snap-Fit Connectors: While the ball and socket joints allow rotation, the joints must be secured together to prevent separation. Annular snap-fit connectors made with TPU were designed to fit within the ball and sockets (Fig. 2). The connector mating angles are low for easy insertion, but the reverse mating angle is 90°, requiring considerable force to separate the blocks. These flexible connectors do not prevent rotation since the connectors can bend. Connector stiffness relates to anatomical joint stiffness: a solid middle section with bending stiffness of 0.1 Nm/° [10] and rails on the sagittal plane for torsional stiffness.

C. Forefoot-Toes Joint

The toe block uses the same flexible TPU material as the annular connectors. This material enables the hallux to bend, modelling the interphalangeal joints. Separation between the hallux and smaller toes emulates the split-toe provided by the Össur™ prosthetic foot cover model.

The FT connector is fused with the toe segment since both sections require flexibility. The FT connector integrates two cantilever snap-fit locks that can be pushed into a matching hole on the forefoot's distal end (Fig. 4). These locks can bend inward, then snap into place. Leaf-locks keep the snap-fit connectors from retracting, preventing separation once inserted. These two snap-fit connectors are connected via a wide strip that provides a metatarsal phalangeal stiffness of approximately 13.8 Nmm/° [11]. The snap-fit connectors are elevated to provide proper rotation in either direction. The edge is rounded to create smooth rotation.

III. Initial Motion Testing Method

Given that a major design criterion was realistic RoM, initial motion testing was required to validate the design before fabricating the full SLL. Fiducial markers were used to track the relative rotation of each joint, printed into sample testing blocks (Fig. 7). A validated Android smartphone application was used to track AprilTag2 fiducial markers [12]. The application accurately tracks up to four markers simultaneously, measuring marker distance and orientation with less than 1° error in all settings [12]. This application was chosen for its simple functionality and minimal equipment required (a phone stand, cardboard markers, and a smartphone). Fig. 5 shows a typical test setup.

Before fabricating the entire SLL, the joints were sectioned into small blocks with joint geometry preserved. Separate blocks were used to test HM AB-AD and DF-PF, MF AB-AD and DF-PF, HM and MF EVE-INV, SH DF-PF and EVE-INV, and FT DF-PF. Fig. 6 shows MF and FT block models. Fig. 7 shows all four joint test blocks.

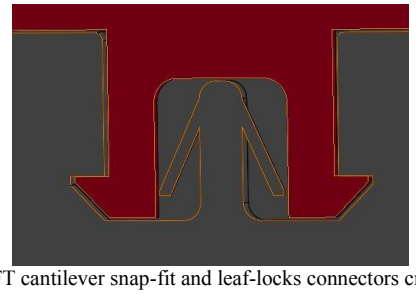

Figure 4. FT cantilever snap-fit and leaf-locks connectors cross-sectional view

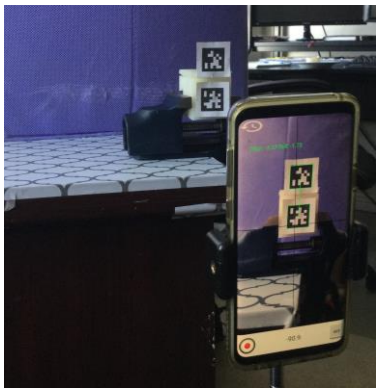

Figure 5. Android smartphone motion test setup

Each test block was leveled with the ground and secured in a vice, with the male section free to move. A smartphone was set up on a tripod at the height of the block, portrait orientation and back camera facing and close to the block to increase marker size within the camera frame (Fig. 5).

An AprilTag2 marker was attached to the section held in the vice and another marker was attached to the free-moving male section. Blocks were leveled and markers were aligned to the leveled edges. For all three planes (frontal, sagittal, transverse), each block was rotated clockwise for 5 s, then released for another 5 s, allowing the block to return to a neutral position. Then the blocks were rotated counter-clockwise for 5 s, then released again for 5 s. The rotations were induced by hand. This cycle was performed three times for each joint. The SH joint tests were slightly different because the ball stud did not have a neutral resting position. Therefore, the ball stud with the marker was held at maximum angle in the clockwise direction, held for 5 s, and then rotated to the maximum angle in the counter-clockwise direction and held for 5 s. The SH cycle was also performed three times.

IV. Results

The motion tracking application produced x and y coordinates for each fiducial marker corner. These coordinates were converted into vector components (v_x, v_y) using (1). One vector was calculated per marker, using the same orientation for each.

$$v_x = x_2 - x_1, v_y = y_2 - y_1 \quad (1)$$

Between the two vectors, v for tag 1 and u for tag 2, the relative angle was calculated using (2). This calculation enabled more direct measurements than the incline angle provided by the app, which provided incline with respect to the phone's gyroscope and not the stationary marker. The angle between bottom vectors of each tag was calculated for each frame. As an example, Fig. 8 shows MF AB-AD angle measurement results.

$$\alpha = \cos^{-1}\left(\frac{(v_x \cdot u_x) + (v_y \cdot u_y)}{\sqrt{v_x^2 + v_y^2} \cdot \sqrt{u_x^2 + u_y^2}}\right) \quad (2)$$

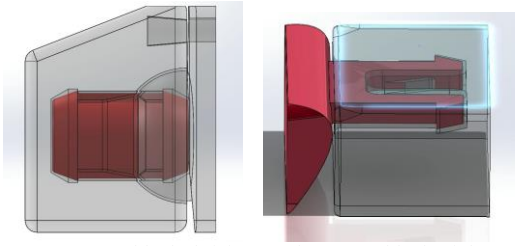

Figure 6. a) MF test block (left image), b) FT test block (right image)

Figure 7. SH, HM, MF, and FT 3D printed test blocks

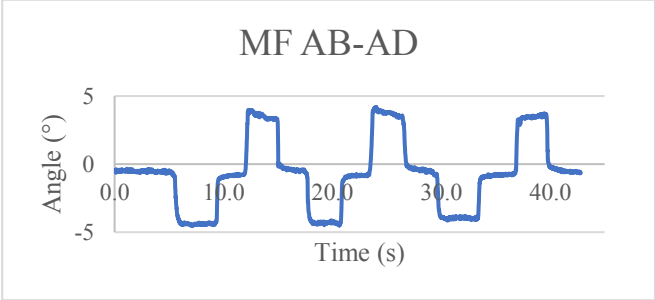

Figure 8. Measured MF transverse rotation angle

Because the load was applied by hand, induced rotation was not always steady (Fig. 8). As such, angles in each position were averaged over 50 frames to remove small variance created by the applied load. Only one angular motion was calculated per tag pair to reduce the noise created by each vector. The difference between the neutral position and rotated position gave the relative rotation angle between fiducial markers. SH measurements did not include a neutral position since the ball stud does not return to a rest position naturally. As such, measurements were taken from one planar maximum to the other. SH results show combined DF-PF and EVE-INV. Each set of averaged values over 50 frames were further averaged into one overall value for each direction, as tabulated in TABLE II. to TABLE V.

TABLE II. SH Reference vs Measured Rotation

	Reference	Measured	Difference
Frontal	50.0°	60.0°	10.0°
Sagittal	70.0°	57.4°	-12.6°

TABLE III. HM Reference vs Measured Rotation

	Reference	Measured	Difference
Eversion	3.5°	5.4°	1.9°
Inversion	3.2°	3.8°	0.6°
Dorsiflexion	2.2°	3.1°	0.9°
Plantarflexion	2.2°	2.6°	0.4°
Abduction	0.5°	1.1°	0.6°
Adduction	3.8°	4.9°	1.1°

TABLE IV. MF IDEAL VS MEASURED ROTATION

	Ideal	Measured	Difference
Eversion	3.5°	3.3°	-0.2°
Inversion	7.0°	6.8°	-0.2°
Dorsiflexion	6.5°	4.9°	-1.6°
Plantarflexion	6.1°	2.9°	-3.2°
Abduction	2.0°	3.8°	1.8°
Adduction	6.5°	4.3°	-2.2°

TABLE V. FT IDEAL VS MEASURED ROTATION

	Ideal	Measured	Difference
Dorsiflexion	80°	80.3°	0.3°
Plantarflexion	30°	31.2°	1.2°

V. DISCUSSION

Most joint angles were within 1° of the desired RoM. However, MF-PF MF-AD, and HM-EVE had differences that were approximately half the target rotation angle. SH motion in both planes had large differences compared to other joints. Both planar motions have a difference of at least 10° from the anatomical target, much greater than other deviations.

The main source of error was the inherent dimensional variance of FDM prints. FDM filaments are applied layer by layer, extruded from a semi-liquid state. While a layer cools, the material can shrink or warp, creating dimensional inaccuracies [13]. The dimensional changes affect RoM since maximum joint rotation angles are controlled by print geometry. However, even with only one initial block for each joint, most HM and MF joints had RoM within 1° of the target values, easily within human variability. As such, the initial concept was validated, justifying the further development of the entire SLL. To improve MF-PF and MF-ADD discrepancies, greater tolerance could be obtained via post-manufacturing processes (e.g. polishing).

SH joint angle discrepancies were related to the small amount of material securing the ball stud in the socket. High RoM requirements for this joint, along with the ball and neck diameter of readily available ball studs, create a situation where a limited amount of material is available to secure the ball stud within the heel plate's upper socket area. As such, the ball stud can extend beyond the theoretical maximum RoM when enough force is applied, possibly dislocating the ball from the socket. Since re-insertion is easy and the SLL will be attached to an AFO during testing, the AFO itself would restrict ankle joint over extension and prevent dislocation.

VI. CONCLUSION AND FUTURE WORK

The SLL joints performed well, rotating within the range of human movement variability. Choosing FDM increases the design's ease of fabrication, but creates dimensional inaccuracies within parts, affecting RoM consistency. Testing showed that the dislocating ball stud creates a limitation for the ankle joint design. However, under normal testing conditions, this issue should be mitigated. Overall, RoM of every joint is within the expected standard deviation for human variability, demonstrating the design's feasibility.

Future research and development will involve fabricating and testing the full SLL assembly to ensure that the RoM is not impacted by other factors. The foot portion of the SLL will then be cast in silicone rubber to emulate soft tissue. Further motion testing will be performed to ensure that the silicone rubber does not restrict joint RoM.

ACKNOWLEDGMENT

The authors would like to thank Joongho Kim for his assistance with FDM printing, providing FDM equipment and expertise for this project. Furthermore, the authors thank Össur for providing a prosthetic foot shell model. This project was funded by NSERC.

REFERENCES

[1] Lemaire, E., 2016, "Mobilizing Knowledge: The Evidence Gap for Assistive Devices," Technology Innovation Management Review, **6**(9), pp. 39–45.

[2] Kobayashi, T., Leung, A. K. L., and Hutchins, S. W., 2011, "Techniques to Measure Rigidity of Ankle-Foot Orthosis: A Review," The Journal of Rehabilitation Research and Development, **48**(5), p. 565.

[3] "Computational and Experimental Evaluation of the Mechanical Properties of Ankle Foot Orthoses: A Literature Review - Alessio Ielapi, Malcolm Forward, Matthieu De Beule, 2019" [Online]. Available: https://journals.sagepub.com/doi/full/10.1177/0309364618824452?casa_token=JsII2uYzNNkAAAAA%3AvwUg_jicBJ5Iavnw8tYaMCHmbJ_M1mN4TdlsPz6wheJFOhzDy4rW7-L7lpLVo9Mx7C1NTiN7fSQ5gQ. [Accessed: 15-Sep-2020].

[4] DeToro, W., 2001, "Plantarflexion Resistance of Selected Ankle-Foot Orthoses: A Pilot Study of Commonly Prescribed Prefabricated and Custom-Molded Alternatives," Jpo Journal of Prosthetics and Orthotics, **13**(2), pp. 39–44.

[5] Wach, A., 2015, "Mechanical Characterization of Carbon Fiber and Thermoplastic Ankle Foot Orthoses," Master's Theses (2009 -).

[6] Nester, C. J., Liu, A. M., Ward, E., Howard, D., Cocheba, J., and Derrick, T., 2010, "Error in the Description of Foot Kinematics Due to Violation of Rigid Body Assumptions," Journal of Biomechanics, **43**(4), pp. 666–672.

[7] Leardini, A., Benedetti, M. G., Berti, L., Bettinelli, D., Nativo, R., and Giannini, S., 2007, "Rear-Foot, Mid-Foot and Fore-Foot Motion during the Stance Phase of Gait," Gait & Posture, **25**(3), pp. 453–462.

[8] 2018, "Strength to Cost Ratio Analysis of FDM Nylon 12 3D Printed Parts," Procedia Manufacturing, **26**, pp. 753–762.

[9] W.c.h., P., H.j., C., and C., S., 2012, "Calculating the Axes of Rotation for the Subtalar and Talocrural Joints Using 3D Bone Reconstructions," Journal of Biomechanics, **45**(6), pp. 1103–1107.

[10] Trevino, S. G., Buford, W. L., Nakamura, T., Wright, A. J., and Patterson, R. M., 2004, "Use of a Torque-Range-of-Motion Device for Objective Differentiation of Diabetic from Normal Feet in Adults," Foot Ankle Int., **25**(8), pp. 561–567.

[11] Heng, M. L., Chua, Y. K., Pek, H. K., Krishnasamy, P., and Kong, P. W., 2016, "A Novel Method of Measuring Passive Quasi-Stiffness in the First Metatarsophalangeal Joint," J Foot Ankle Res, **9**(1), p. 41.

[12] Basiratzadeh, S., Lemaire, E. D., Dorrikhteh, M., and Baddour, N., 2019, "Fiducial Marker Approach for Biomechanical Smartphone-Based Measurements," *2019 3rd International Conference on Bio-Engineering for Smart Technologies (BioSMART)*, pp. 1–4.

[13] "Dimensional Accuracy of 3D Printed Parts," 3D Hubs [Online]. Available: https://www.3dhubs.com/knowledge-base/dimensional-accuracy-3d-printed-parts/. [Accessed: 22-Feb-2021].